Topics in Catalysis
https://doi.org/10.1007/s11244-022-01758-4

ORIGINAL PAPER

NH_3-NO SCR Catalysts for Engine Exhaust Gases Abatement: Replacement of Toxic V_2O_5 with MnO_x to Improve the Environmental Sustainability

L. Consentino[1] · Giuseppe Pantaleo[1] · V. La Parola[1] · C. Migliore[1] · E. La Greca[1] · Leonarda Francesca Liotta[1]

Accepted: 24 November 2022

Abstract
Mn-WO_3/TiO_2 catalysts were investigated for Selective Catalytic Reduction (SCR) of NO with NH_3. The catalysts were synthesized by wetness impregnation method with different Mn loadings (1.5-3-12 wt%) on 8wt%WO_3/TiO_2. All three catalysts were compared with 8wt%WO_3/TiO_2 and bare MnO_x oxide, used as references. The 1.5wt%Mn-8wt%WO_3/TiO_2 exhibited the highest performance in NO conversion and N_2 selectivity. A commercial catalyst, based on titania supported vanadia and tungsta, (V_2O_5-WO_3/TiO_2), widely used for its high efficiency, was also investigated in the present work. The morphological, structural, redox and electronic properties of the catalysts and their thermal stability were studied by several techniques (N_2 adsorption/desorption, X-ray diffraction, H_2 temperature-programmed reduction, NH_3 temperature programmed desorption, X-ray photoelectron spectroscopy).

The aim of this paper is to study the effect of different Mn loadings on 8wt%WO_3/TiO_2 with the ambition to obtain highly active and selective catalysts in a large window of temperature. The replacement of toxic vanadium used in the classic V_2O_5-WO_3/TiO_2 catalyst with MnO_x in the best performing catalyst, 1.5wt%Mn-8wt%WO_3/TiO_2, represents an important achievement to improve the environmental sustainability.

Keywords NH_3-SCR · Manganese oxide · Tungsten oxide · Vanadium free catalyst

1 Introduction

Nitrogen oxides (NO_x) emitted by mobile and stationary sources are one of the major causes of air pollution and are responsible for a series of environmental problems such as acid rain, photochemical smog and the green-house effect [1]. In recent years the low temperature (100–200 °C) selective catalytic reduction (SCR) of NO_x by NH_3 has been investigated and metal doped titanates have attracted attention, for controlling NO_x emissions from stationary sources, thanks to their elevated performances and low cost [2]. Among common catalytic devices for NO SCR in stationary plants, V_2O_5-WO_3/TiO_2 catalysts are used, however, some problems remain due to the high activity for oxidation of SO_2 to SO_3, the rapid decrease in activity and selectivity above 550 °C, and the toxicity of the vanadium pentoxide due to easy sublimation [3, 4]. So, NO SCR devices used in stationary sources must be installed upstream the particulate collector and flue gas desulfurization in order to meet the optimum working temperature of 350–400 °C. On the other hand, for mobile sources, this type of V_2O_5-WO_3/TiO_2 catalyst is not the best solution for diesel engine exhaust gases aftertreatment, as it cannot completely remove NO_x due to the wide temperature window of exhaust gas (150–500 °C). Therefore, researchers in the field of academia and industry continue to develop new low-temperature catalysts that can work well around 250 °C.

It is well known that the nature of the catalyst is crucial for an efficient SCR of NO_x by NH_3 or urea. Transition metal oxides including iron (Fe), manganese (Mn), cerium (Ce), copper (Cu) and nickel (Ni) have been, recently, investigated showing extraordinary catalytic performance

✉ Giuseppe Pantaleo
giuseppe-pantaleo@cnr.it

✉ Leonarda Francesca Liotta
leonardafrancesca.liotta@cnr.it

[1] Institute for the Study of Nanostructured Materials (ISMN)-CNR, via Ugo La Malfa, 153, 90146 Palermo, Italy

for NO_x removal. In particular, Mn-based catalysts reported both, high NO conversion and N_2 selectivity at low temperature [3, 4] since manganese oxide contains different types of labile oxygen, as described by Kapteijn et al. [5]. Nevertheless, the application of pure MnO_x is not recommended due to its low surface area and poor thermal stability [6]. For such reasons, supported MnO_x on Al_2O_3 [7], TiO_2 [8], USY [9], MnO_x/AC [10] and MnO_x/ACF [11] have been developed. Among these, MnO_x/TiO_2 exhibited the best performance at low temperature [4]. It has been also considered the opportunity to dope TiO_2 -supported manganese catalysts with transitional metal in order to evaluate combined effects between the two metal oxides. For example, Fe_2O_3, WO_3, MoO_3, and Cr_2O_3 were investigated by Wu et al. [12] finding that Mn-W/TiO_2 showed the higher NO_x conversion followed by Mn-Fe/TiO_2, Mn-Cr/TiO_2 and Mn-Mo/TiO_2.

Tungsten oxide is well-known for promoting the activity and stability of the commercial vanadium-based catalyst (V_2O_5-WO_3/TiO_2). WO_3 forms W-Ti-O chemical bonds over TiO_2 surface [13] and stabilize anatase phase of TiO_2 giving high thermal stability to the catalyst [14–16]. In addition, as Shan et al. reported, tungsten increases both the surface Brönsted and Lewis acidity and the operation temperature window of SCR [17]. Therefore, binary metal oxide-based catalysts, as MnO_x-WO_3/TiO_2, are noteworthy for low temperature NO SCR.

In this work we have investigated Mn-WO_3/TiO_2 catalysts synthesized by wetness impregnation to evaluate the effect of Mn loading on the activity and selectivity in NO conversion with the aim to extend the window of operating temperature. Moreover, we have compared the best catalyst with a commercial SCR device, based on V_2O_5-WO_3/TiO_2, in order to replace the harmful vanadium pentoxide with Mn, preserving high efficiency in NO_x removal. The physical-chemical, structural and surface properties of the catalysts have been investigated by XRD, BET, H_2-TPR, NH_3-TPD, XRD and XPS techniques.

2 Experimental

2.1 Catalyst Preparation

All reagents were analytical grade and used as received without further purification. Firstly, we prepared the 8wt% WO_3/TiO_2 oxide (WTi) by wetness impregnation method of a commercial TiO_2 oxide, like P25 (provided by Sigma-Aldrich). A proper amount of $(NH_4)_{10}H_2(W_2O_7)_6$ was mixed with oxalic acid solution with a molar ratio of the acid to paratungstate equal to 8:1. This solution was added dropwise to the TiO_2 support. Subsequently, the obtained paste was dried overnight at 120 °C and calcined at 400 °C for 2 h in static air. A certain amount of TiO_2 (Sigma-Aldrich) was calcined in the same conditions and used as reference. The WTi oxide was impregnated, by wetness impregnation method, with few mL of an aqueous solution of $Mn(NO_3)_2.xH_2O$, in appropriate concentration in order to prepare catalysts with three Mn loadings, corresponding to 1.5, 3.0 and 12.0 wt% as Mn. After drying overnight at 120 °C, calcination was carried out at 400 °C for 2 h. The so prepared materials were labelled as xMnWTi (x = 1.5, 3, 12). Bare MnO_x oxide was prepared starting from 0.5 M $Mn(NO_3)_2.xH_2O$ solution by precipitation with 0.5 M Na_2CO_3 solution. After drying at 120 °C, calcination at 400 °C for 4 h was performed.

Table 1 Chemical composition of the prepared samples and relative labels

Sample	Label
Bare MnO_x	MnO_x
TiO_2 calcined	TiO_2 calc.
8wt% WO_3/TiO_2	WTi
1.5wt% Mn-8wt% WO_3/TiO_2	1.5MnWTi
3wt% Mn-8wt% WO_3/TiO_2	3MnWTi
12wt% MnO_2-8wt% WO_3/TiO_2	12MnWTi
3wt%V_2O_5-7wt%WO_3/75wt%TiO_2-6wt% bentonite-9wt% glass fiber	VWTi

A commercial catalyst (VWTi), provided by Hug Engineering (ElringKlinger Group), with composition 3wt% V_2O_5-7wt% WO_3/75wt% TiO_2-6wt% bentonite- 9wt% glass fiber was used as reference. Details about chemical physical properties were reported elsewhere by some of us [18].

All the samples and their relative labels are listed in Table 1.

2.2 Catalysts Characterizations

Elemental analysis of the catalysts was carried out by Atomic Emission Spectroscopy (MP-AES 4200 Agilent technologies), after treatment in acidic solution with H_2SO_4 and HNO_3 at 250 °C for complete dissolution. The real chemical composition corresponded well to the nominal one within ± 5%.

Specific surface areas (SSA) and pore volumes were determined by N_2 adsorption –desorption isotherms at -196 °C using a Micromeritics ASAP 2020 equipment, through Brunauer –Emmett-Teller (BET) method in the standard pressure range 0.05–0.3 P/P^0. Before the measurements, the samples were degassed at 250 °C for 2 h. By analysis of the desorption curves, using the Barrett–Joyner–Halenda (BJH) method the pore volume and pore size distribution were obtained.

X-ray diffraction (XRD) patterns were acquired with a Bruker goniometer employing Ni-filtered Cu Kα radiation. A proportional counter and 0.05° step size in 2θ were used.

The assignment of the crystalline phases was based on the JPDS powder diffraction file cards [19].

Temperature programmed desorption of ammonia (NH_3-TPD) was performed using the Micromeritics Autochem 2910 equipped with an ultraviolet gas analyzer (ABB, Limas 11). Before starting the ammonia adsorption experiment, the sample was pre-treated in He flow at 200 °C for 30 min. After cooling to room temperature, a stream of 5% NH_3/He (30 mL/min) was flowed over the sample for 1 h. To remove the physically adsorbed ammonia, the sample was purged in flowing He (100 mL/min) at 100 °C for 1 h. Then, cooling down to room temperature, ammonia desorption was monitored with the UV gas analyser, flowing He (30 mL/min) and heating up to 600 °C (rate of 10 °C/min), holding time at 600 °C for 30 min. Before the gas detection system, a cold trap was used to condense any water desorbed from the sample. The ammonia concentration, in terms of ppm NH_3 desorbed/g_{cat} under He flow (30 mL/min) was plotted versus time and temperature.

The X-ray photoelectron spectroscopy (XPS) analyses were performed with a VG Microtech ESCA 3000 Multilab, equipped with a dual Mg/Al anode. As excitation source was used the Al Kα radiation (1486.6 eV). The sample powders were mounted on a double-sided adhesive tape. The pressure in the analysis chamber was in the range of 10^{-8} Torr during data collection. The constant charging of the samples was removed by referencing all the energies to the C 1s binding energy set at 285.1 eV. Analyses of the peaks were performed with the CasaXPS software.

Hydrogen temperature programmed reduction (H_2-TPR) measurements were carried out with a Micromeritics AutoChem 2910 HP Automated Catalyst Characterization System, equipped with a thermal conductivity detector (TCD). An amount of 0.1 g of sample was used for each analysis. The samples were pre-treated with a mixture of 5%vol. O_2 in He, at a flow rate of 50 mL/min, heating up (10 °C/min) up to 400 °C and holding at this temperature for 30 min. After cooling down to room temperature under He flow, the gas mixture with composition 5%vol. H_2 in Ar was flowed at 30 mL/min into the sample tube. During the analysis, the temperature was increased up to 1000 °C at a rate of 10 °C/min.

2.3 Catalysts Activity test

NO SCR by NH_3 tests were performed in a fixed-bed U quartz reactor with an inner diameter of 12 mm. The feed gas, consisting of 1000 ppm NO, 1000 ppm NH_3, 10%vol. O_2 and He as balance, was led over the catalyst (60 mg) at a flow rate of 50 mL/min (STP), equivalent to a gas hourly space velocity (GHSV) of 50,000 h^{-1}. The activities were measured as a function of temperature heating from 25 to 400 °C with steps of 25–50 °C and the data were collected after about 40 min at each temperature, in order to achieve steady-state conditions. The inlet and outlet gas compositions were analyzed by ABB detectors, infrared (Limas 11) for NO, N_2O, NO_2, NH_3, paramagnetic (Magnos 206) for O_2. The NO conversion and N_2 selectivity [20] were calculated by the following equations:

$$NO\ Conversion\,\% = \frac{[NO]_{in} - [NO]_{out}}{[NO]_{in}} \times 100$$

$$N_2\ Selectivity\,(\%) = \left[1 - \frac{[NO_2]_{out} + 2[N_2O]_{out}}{[NO]_{in} + [NH_3]_{in} - [NH_3]_{out} - [NO]_{out}}\right] \times 100$$

Table 2 Morphological parameters of the prepared catalysts

Samples	Surface area ($m^2\ g^{-1}$)	BJH Pore Volume (cm^3 /g)	Mean Pore Diameter (nm) by BJH Method
MnO_x	119.1	0.36	10.9
TiO_2	56.0	0.28	21.1
TiO_2 calc.	52.0	0.27	22.1
WTi	61.7	0.47	29.2
1.5MnWTi	74.4	0.50	26.3
3MnWTi	75.9	0.48	25.3
12MnWTi	72.0	0.40	22.1
VWTi	55.6	0.21	15.0

3 Results and Discussion

3.1 Catalysts Characterization

3.1.1 BET and XRD Analyses

In Table 2 the morphological properties of the different catalysts are listed. As shown, the MnO_x exhibited the highest surface area (119.1 m^2/g), pore volume (0.36 cm^3/g) and mean pore size around 11 nm. The surface area of as received TiO_2 was 56 m^2/g, slightly decreasing to 52 m^2/g after calcination. No significant changes occurred in the pore volume and mean pore size that remained around 0.27 cm^3/g and 22.0 nm, respectively.

The WO_3 loading on TiO_2 produced some changes in the morphology by increasing its porosity (pore volume 0.47 cm^3/g, pore size 29.2 nm) and surface area (61.7 m^2/g). A similar trend occurred after the impregnation of manganese on the WTi oxide, for which SSA increased until 3wt% of manganese loading, while almost stable pore volume and mean pore size values were registered in comparison with the parent WTi. Such findings suggest high dispersion of amorphous MnO_x up to a loading of 3wt% in good accordance with the absence of crystalline phases for all

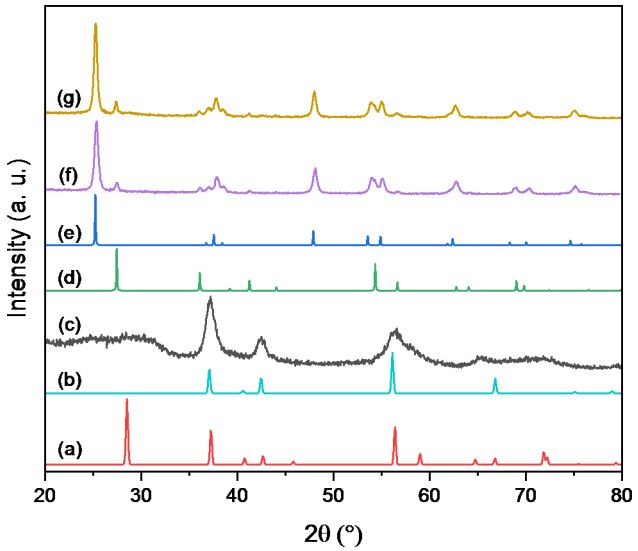

Fig. 1 XRD patterns of (a) MnO_2 (#759,758), (b) MnO_2 (#29,561), (c) MnO_x, (d) TiO_2 rutile (#9161), (e) TiO_2 anatase (#9854), (f) WTi and (g) 12MnWTi

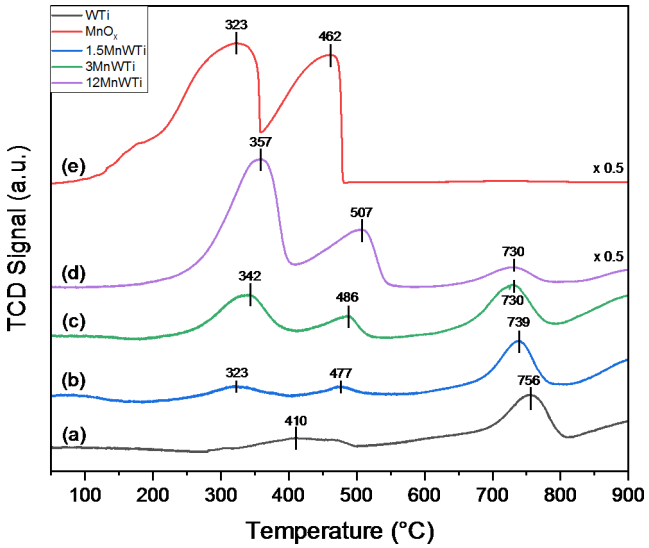

Fig. 2 H_2-TPR profiles of (a) WTi, (b) 1.5MnWTi, (c) 3MnWTi, (d) 12MnWTi and (e) MnO_x

xMnWTi catalysts, as reported in the XRD results. As far as 12MnWTi the SSA decreased in comparison with 1.5 MnWTi and as well the pore volume and mean pore size decreased, implying that some agglomeration of manganese oxide on the surface of the catalyst may occur (see also XPS characterization).

The reference commercial catalyst, VWTi, has SSA 55.6 m^2/g, pore volume 0.21 cm^3/g and mean pore size 15 nm [18].

Figure 1 displays the XRD patterns of 12MnWTi, WTi, pure MnO_x and the corresponding ICSD references. Regarding the bare MnO_x, the intense peaks at $2\theta = 37.1° - 42.4° - 56.1° - 66.8°$ were ascribed to MnO_2 mainly as hexagonal phase (ICSD #29,561), though the coexistence of tetragonal phase (ICSD #759,758) cannot be excluded due to quite broad and weak peak around $2\theta = 28.5° - 71.8°$. In the case of WTi the sharp peaks were attributed to the anatase (ICSD #9854) and rutile (ICSD #9161) phases of titania, while no peaks corresponding tungsten oxide were observed, indicating the highly dispersion of the WO_3 on the surface. Compared with the pattern of WTi, the deposition of Mn did not produce any new crystalline phase, no characteristic peaks of MnO_2 were detected even at high loading (12MnWTi). As far as the VWTi reference, only peaks of the anatase phase were identified [18], being a commercial catalyst likely deposited over a less common titania.

3.1.2 H_2-TPR

The reducibility of xMnWTi samples was investigated by H_2-TPR experiments. Corresponding analyses were also performed on MnO_x and WTi used as reference materials. The H_2-TPR profiles of MnO_x, WTi, and xMnWTi catalysts are shown in Fig. 2 and the theoretical and experimental H_2 consumption values (mL/g) are listed in Table 3.

As reported in the literature, the MnO_x reduction can occur through two-step process $MnO_2 \rightarrow Mn_2O_3 \rightarrow MnO$ [21, 22] according to the shape of the curve. In fact, two strong peaks at 323 and 462 °C with a slight shoulder at around 170 °C were observed for MnO_x, corresponding to the stepwise reduction above mentioned. Moreover, according with the literature, the shoulder reduction peak can be attributed to reducible small clusters of surface manganese oxide species [21]. Assuming that all manganese is present as MnO_2, the theoretical hydrogen consumption requested for the reduction of Mn^{4+} to Mn^{2+} is equal to 281 mL/g (Table 3). Being the experimental consumption equal to 210 mL/g it can be deduced that in the bulk MnO_x the manganese species are present mainly as Mn^{4+} along with Mn^{3+}, as confirmed by XPS results. In accordance with this result, it was proposed that MnO_2 and Mn_2O_3 are the primary active phases for NO reduction in MnO_x catalysts for SCR reaction, especially MnO_2 [23].

The TiO_2 hydrogen consumption reported in Table 3 refers to the titania oxide that was calcined under the same conditions as for MnWTi catalysts. H_2-TPR of WTi catalyst (Fig. 2) showed an intense peak at 756 °C related to the reduction of W^{6+} to W^{4+} [24]. The reduction peak at 410 °C corresponds to the surface reduction $Ti^{4+} \rightarrow Ti^{3+}$ while the reduction of bulk titanium occurs at high temperature (over 800 °C) [25–27].

After the deposition of bare MnO_x on WTi, the reduction peaks associated to MnO_x in 1.5-3-12MnWTi catalysts were shifted progressively at higher temperature indicating that MnO_x strongly interacts with the support and is less easy to

Table 3 Theoretical and experimental H_2 consumption (mL/g) of catalysts calculated by TPR analyses

Catalyst	Reduction steps	Theoretical H_2 Volume (mL/g)	Experimental H_2 Volume (mL/g)
MnO_x	$Mn^{4+} \rightarrow Mn^{2+}$	281	210
TiO_2	$Ti^{4+} \rightarrow Ti^{3+}$	-	9
WTi	$W^{6+} \rightarrow W^{4+}$	9	
	$Ti^{4+} \rightarrow Ti^{3+}$	8	
	Total	17	17
1.5MnWTi	$Mn^{3+} \rightarrow Mn^{2+}$	3	
	$W^{6+} \rightarrow W^{4+}$	8	
	$Ti^{4+} \rightarrow Ti^{3+}$	8	
	Total	19	19
3MnWTi	$Mn^{3+} \rightarrow Mn^{2+}$	6	
	$W^{6+} \rightarrow W^{4+}$	8	
	$Ti^{4+} \rightarrow Ti^{3+}$	8	
	Total	22	22
12MnWTi	$Mn^{3+} \rightarrow Mn^{2+}$	25	
	$W^{6+} \rightarrow W^{4+}$	7	
	$Ti^{4+} \rightarrow Ti^{3+}$	7	
	Total	39	39

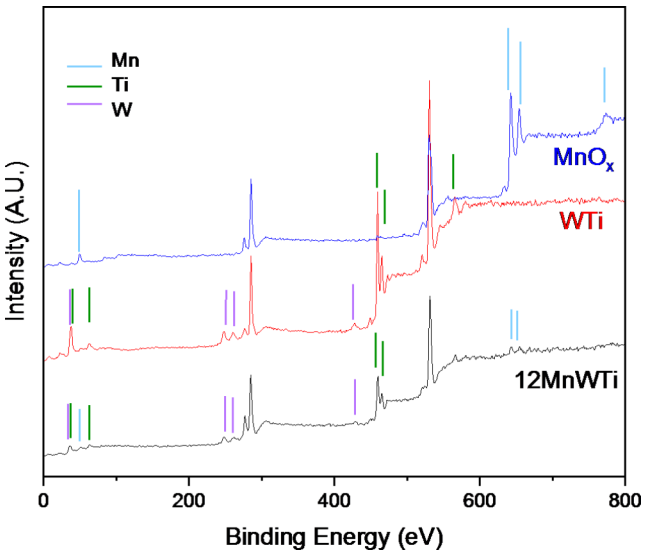

Fig. 3 Survey spectra of MnO_x, WTi and 12MnWTi

reduce. In good accordance with the theoretical and experimental total hydrogen consumption values (see Table 3), manganese was stabilized as Mn^{3+} over WTi oxide, according to XPS data, and completely reduced to Mn^{2+}.

3.1.3 XPS Analyses

X ray Photoelectron Spectroscopy has been used to evaluate the changes occurring upon deposition of manganese and tungsten oxides on the titania surface. Figure 3 shows the survey spectra of MnO_x, WTi and 12MnWTi. Besides the peaks due to C1s, arising by atmospheric contamination,

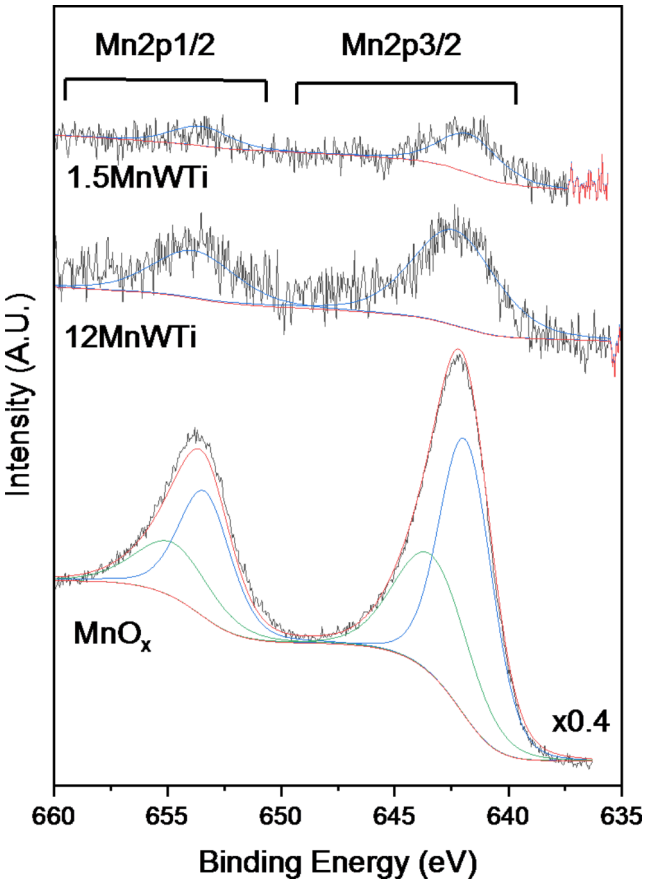

Fig. 4 Mn 2p region for MnO_x, 1.5MnWTi and 12MnWTi

Table 4 Mn $2p_{3/2}$, W $4f_{7/2}$ binding energy (eV). W/Ti and Mn/Ti atomic ratio

Samples	Mn $2p_{3/2}$[a]	W $4f_{7/2}$	W/Ti (0.03)[b]	Mn/Ti[b]
MnO_x	641.9 (62%) 643.4 (38%)	-	-	-
WTi	-	35.7	0.10	-
1.5MnWTi	641.7 (100%)	35.8	0.11	0.04 (0.02)
12MnWTi	642.4 (100%)	35.9	0.15	0.19 (0.24)

[a] in parenthesis the relative percentage of the different components is reported

[b] in parenthesis the theoretical atomic ratio is listed

only peaks due to Mn, Ti, W and O are visible on the surface, indicating that no precursor residues are present in the samples. Figure 4 shows the high-resolution region of Mn 2p for MnO_x, 1.5MnWTi and 12MnWTi with the two components of Mn $2p_{3/2}$ and Mn $2p_{1/2}$ separated by 11.5 eV. In Table 4 the binding energies corresponding to Mn $2p_{3/2}$ are reported. Mn $2p_{3/2}$ component for MnO_x can be deconvoluted with two peaks at 641.9 eV and 643.4 eV which can be

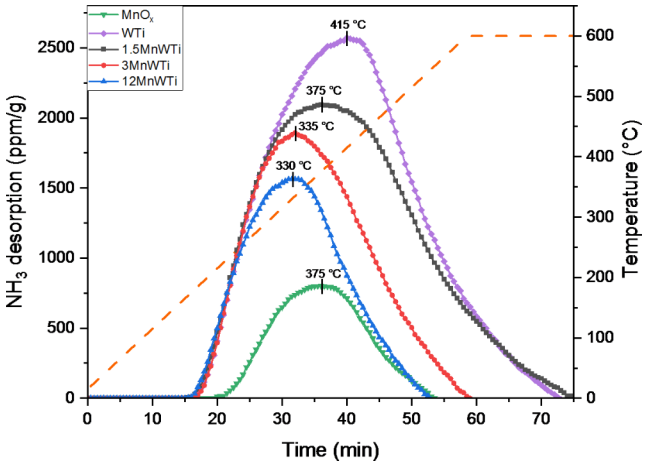

Fig. 5 NH_3-TPD curves of catalysts as function of time and temperature

Table 5 Acidic properties of the prepared catalysts determined by NH_3-TPD.

Samples	Temperature range (°C)	NH_3 uptake (μmol g^{-1})	Surface acidity density (μmol NH_3 g^{-1} m^{-2})
MnO_x	215–545	18	0.15
WTi	175–600	89	1.44
1.5MnWTi	175–600	79	1.06
3MnWTi	175–600	52	0.68
12MnWTi	175–545	38	0.53

attributed to Mn (III) and Mn (IV) respectively [28, 29]. The deposition of MnO_x on WTi stabilizes Mn (III) oxidation state as evidenced by the position of the peaks (see Fig. 4; Table 4) in both 1.5 and 12MnWTi. Tungsten position of W $4f_{7/2}$ is, for all samples, indicative of W (VI) [30–32]. Table 4 shows also the surface atomic ratios. Generally, the ratio measured is higher than the theoretical one, in accord with the fact that both W and Mn have been introduced by impregnation and are therefore localized on the surface. As far as 12MnWTi the surface Mn/Ti ratio is lower than the theoretical one and this is probably due to the high amount of Mn leading to the formation of some agglomerated particles. By looking at W/Ti surface atomic ratio it seems that the deposition of manganese occurs preferentially on titanium, as evidenced by the relative increase of the W/Ti with the increase of MnO_x on the sample.

3.1.4 NH_3 – TPD Analyses

The surface acidity properties of 1.5-3-12MnWTi and those of the bare MnOx and WTi oxides were investigated by NH_3-TPD analyses. The ammonia desorption curves of all catalysts are shown in Fig. 5 and ammonia uptakes are reported in Table 5. All the catalysts exhibited ammonia desorption within the temperature range of 175–600°C. The temperature of the desorption peak maxima gives indications about the nature and the relative strength of acidic sites, while the area under the ammonia desorption represents the number of surface acidic sites. The acid site density was also calculated (see Table 5) by dividing the ammonia uptake by the catalysts surface area. Among the analysed samples, the WTi was characterized by the highest acidity, conversely the bare MnO_x showed very low acidic behavior.

The so far reported data are in good agreement with our review article [33] where we reported that tungsten plays a considerable role increasing Brönsted and Lewis acidic sites. The number of acidic sites and acidic density exhibited the following order MnO_x < 12MnWTi < 3MnWTi < 1.5MnWTi < WTi. As discussed in NH_3-SCR performance section, by increasing manganese loading over WTi, the surface acidity promoted by tungsten oxide decreased and consequently the catalysts exhibited high activity in the low temperature range. Conversely, at low manganese loading the acidity of WTi was scarcely influenced resulting in high NO conversion of catalysts at high temperature. Summarizing, the manganese loading deposited over the surface of WTi played the key role of acidity moderator for the tungsten-based catalyst, influencing the catalytic properties of the MnWTi samples that exhibit tailored NO SCR activity at low, medium or high, temperatures.

3.1.5 NO SCR by NH_3 Catalytic Performances

Figures 6 and 7 show the NO conversion and N_2 selectivity curves for the prepared catalysts and the commercial reference, VWTi. Pure MnO_x was able to achieve considerable conversion values, above 80–90% at low temperature, in the range 100–200 °C. Then, the oxidation of ammonia was promoted at T > 200 °C and the NO SCR collapsed towards almost no conversion at 300 °C.

WTi exhibited a completely opposite trend showing extremely poor activity at low temperature and NO conversion between ~ 70–95% in a restricted range, 350–400 °C. This finding confirmed previous investigations about the relatively low efficiency of only WO_3 based catalysts [34, 35]. Concerning the xMnWTi samples, it was found that the MnO_x loading strongly influenced their catalytic activity. As shown in Figs. 3 and 6MnWTi was the best performing sample with NO conversion values over 80% up to ~ 98% in a wide temperature range, from 150 to 300 °C. In the case of the1.5MnWTi, the NO conversion started to increase at T > 150 °C achieving 92% at 300–350 °C, while the 12MnWTi catalyst reached almost full conversion at 200 °C, with slightly lower values near 90% at 150 and

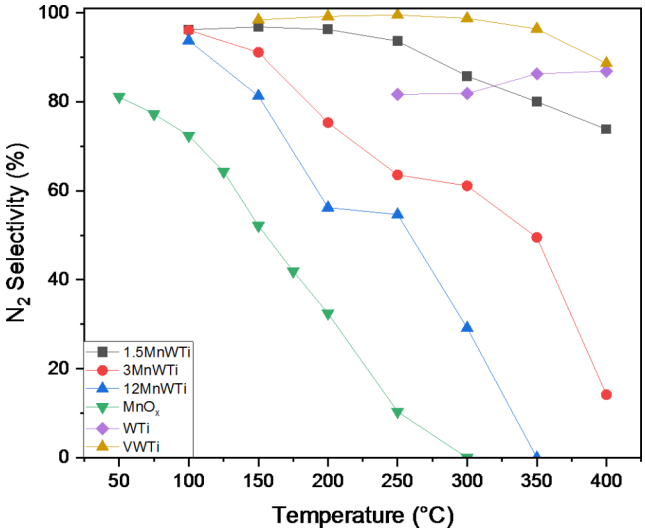

Fig. 7 N_2 selectivity 1.5-3-12MnWTi, MnO_x, WTi and VWTi as reference. Reaction conditions: [NO] = [NH_3] = 1000 ppm, [O_2] = 10 vol% and He as balance at GHSV of 50,000 h^{-1}

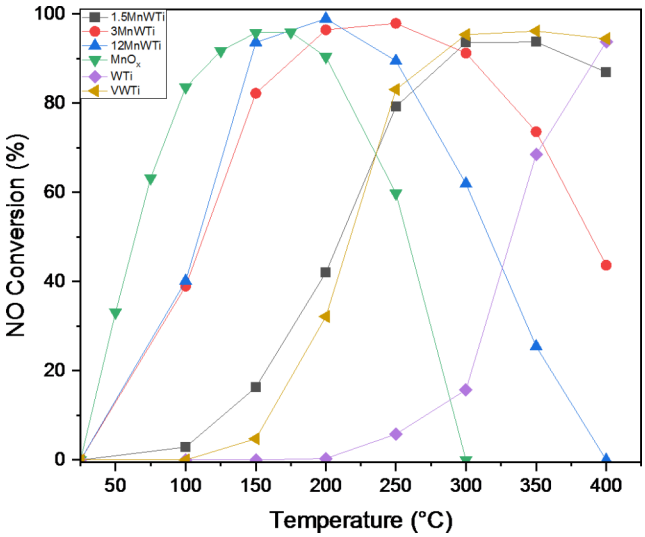

Fig. 6 NO_x conversion 1.5-3-12MnWTi, MnO_x, WTi and VWTi as reference. Reaction conditions: [NO] = [NH_3] = 1000 ppm, [O_2] = 10 vol% and He as balance at GHSV of 50,000 h^{-1}

250 °C, respectively. Based on the so far reported data it results that, as a function of the manganese content, it is possible to modulate the catalytic performances of the MnWTi catalysts in the range of low, medium or high temperature.

As previously discussed, and in agreement with our review [33], tungsten oxide plays a considerable role in NH_3-NO SCR by increasing Brönsted and Lewis acidity and stabilizing against sintering and transition to rutile the anatase phase of TiO_2 that synergically catalyzes the reaction. As reported by Zhu et al. [36] strong Lewis sites are active in the NO SCR at high temperatures (> 350 °C), weak Lewis acid sites contribute at low temperatures (< 200 °C) and Brönsted acid sites promote the conversion at medium temperature (250–300 °C). Therefore, it results that the acidity of the MnWTi catalysts increased or decreased as a function of a different Mn loading that affected the NO conversion efficiency in all range of temperature investigated, between 100 and 400 ° C.

Among all the xMnWTi catalysts, 3MnWTi displayed the highest activity in NOx conversion, but an ideal catalyst is expected to have high N_2 selectivity in order to avoid emission of harmful nitrogen oxides as NO_2 and N_2O [37, 38]. As shown in Fig. 7, the selectivity of MnO_x rapidly declined already at very low temperature, being less than 10% at 250 °C, while the WTi showed almost constant values not higher than 80–85% in the range 250–400 °C.

In the between of the above-mentioned catalysts, there are 12MnWTi and 3MnWTi showing a declining selectivity trend in the whole temperature window (100–400 °C). The 1.5MnWTi exhibited high selectivity, more than 90% up to 250 ° C with values between 80 – 70% at 350–400 °C. Therefore, such catalyst represents the best compromise between good catalytic performance in NO_x conversion at high temperature window (250–400 °C) and high selectivity.

The drop in selectivity observed for MnO_x, 3MnWTi and 12MnWTi catalysts was ascribed to the competitive oxidation reaction of ammonia catalysed by manganese, which produces NO, NO_2 and N_2O and consequently decreased the selectivity [5]. In order to confirm the occurrence of such reaction, in Fig. 8 the NH_3, NO, NO_2 and N_2O concentration (ppm) trends as a function of temperature were compared for two catalysts, the worse selective and the best one, respectively, MnO_x and 1.5MnWTi.

In the case of MnO_x, simultaneously with the decrease in the concentration of NO and NH_3 the signal of N_2O appears, already at 50 °C, and increased with the temperature up to a maximum of ~ 600 ppm at 200–250 °C; then above 250 °C the N_2O values decreased together with the increase of NO_2.

entration (ppm) as a function of temperature for MnO_x (a) and 1.5MnWTi (b) catalysts.

As for the 1.5MnWTi, that among the investigated catalyst is the most selective towards N_2 formation, the NO and NH_3 conversion was accompanied by low N_2O formation and almost no NO_2 was detected.

After identifying the best compromise between catalytic activity and N_2 selectivity in the 1.5MnWTi, we focused on comparing NO conversion and N_2 selectivity curves of such catalyst with those of the commercial reference (VWTi) (see Figs. 6 and 7).

It results that although 1.5MnWTi is less selective than the commercial catalyst, especially above 250 °C, it displayed similar or even enhanced (150–200 °C) NO conversion.

Considering the toxicity and low thermal stability of V_2O_5, that is the active phase in the commercial catalyst

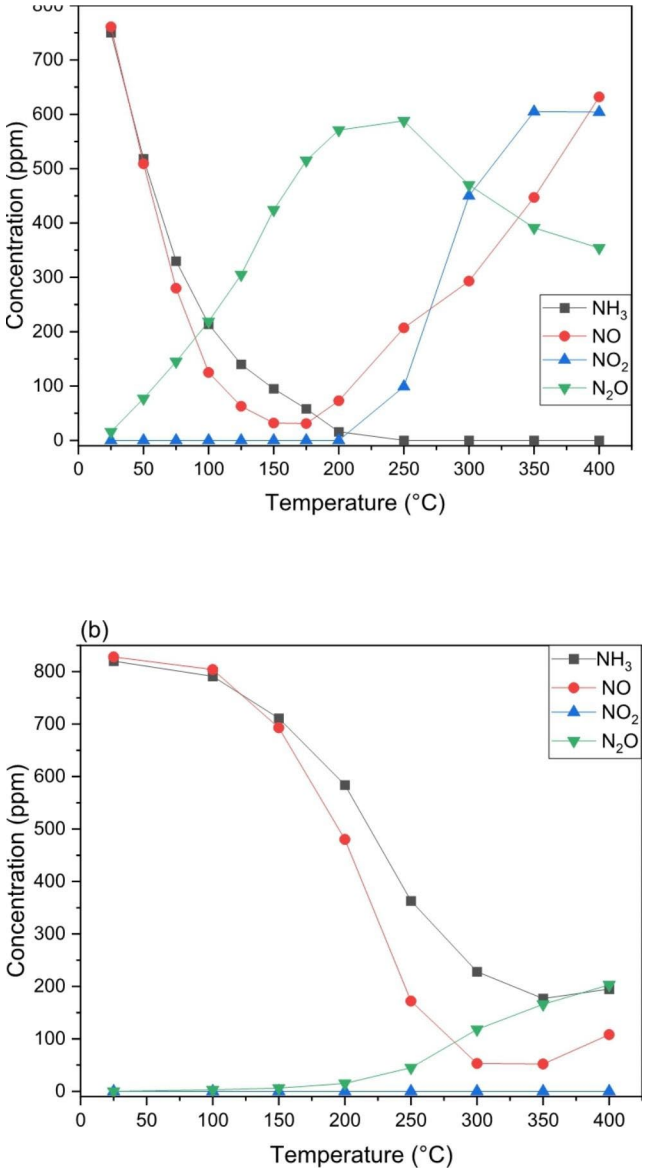

Fig. 8 Comparison of NH_3, NO, NO_2 and N_2O conc

along with WO_3, the good performances achieved by the 1.5MnWTi represent an important result for the improvement of the environmental sustainability of NH_3-NO SCR devices.

4 Conclusion

Different loadings of Mn were successfully deposited by wetness impregnation over WO_3/TiO_2 and the resulting series of xMnWTi catalysts was investigated for SCR of NO by NH_3.

The 3MnWTi catalyst showed the best catalytic activity with NO conversion values over 80% up to ~98% in a wide temperature range, from 150 to 300 °C, although the N_2 selectivity quickly declined to ~60% at 200 °C and even lower at higher temperature. Conversely in the case of the 1.5MnWTi the NO conversion was higher than 90% at 300–350 °C and the selectivity to N_2 varied between 90 – 80% in the range of temperature 100–350 °C. Such sample represents the best compromise between NO conversion and N_2 selectivity.

BET and XRD characterizations revealed that 1.5MnWTi sample had large surface area and well dispersion of tungsten and manganese oxides. The good accordance between H_2 consumption in TPR and XPS data confirmed the presence in the xMnWTi of MnO_2 and Mn_2O_3 that are known as the primary active phases for NO SCR reaction. Surface acidity was influenced by the synergistic effect of tungsten and manganese. The former was able to increase the number of Brönsted and Lewis acidic sites, while the latter modulated the acidity of tungsten-based catalyst and consequently influenced the NO conversion and the selectivity to N_2 of the MnWTi series making them more or less efficient at high, medium or low temperatures. Among the investigated samples, the 1.5MnWTi represents the best composition. Although with a slight decay in N_2 selectivity at temperature above 250 °C, it performed almost as good as the reference commercial catalyst with the great advantage of replacing the toxic V_2O_5 with MnO_x.

Acknowledgements The projects TECBIA "Tecnologie a Basso Impatto Ambientale per la Produzione di Energia sui Mezzi Navali" (Progetto n. F.090041/01/X36 –CUP B98I17000680008)" and the project NAUSICA (PON "R&S 2014–2020", grant n. ARS01_00334); project leader NAVTEC cluster are acknowledged for financial support. The authors are grateful to Ing. L. Pinauda (Hug Engineering AG) for providing the commercial catalyst, to G. Napoli (ISMN-CNR, Italy) for the economic report of the above projects, to F. Giordano (ISMN-CNR, Italy) for XRD and to N. Gallì (ISMN-CNR, Italy) for BET analyses.

References

1. Chen J, Chen Y, Zhou M et al (2017) Enhanced performance of Ceria-Based NO_x reduction catalysts by optimal support effect. Environ Sci Technol 51:473–478. https://doi.org/10.1021/acs.est.6b04050

2. Roy S, Viswanath B, Hegde MS, Madras G (2008) Low-temperature selective catalytic reduction of NO with NH_3 over $Ti_{0.9}M_{0.1}O_{2-\delta}$ (M = cr, Mn, Fe, Co, Cu). J Phys Chem C 112:6002–6012. https://doi.org/10.1021/jp7117086
3. Thirupathi B, Smirniotis PG (2011) Co-doping a metal (Cr, Fe, Co, Ni, Cu, Zn, Ce, and zr) on Mn/TiO_2 catalyst and its effect on the selective reduction of NO with NH_3 at low-temperatures. Appl Catal B Environ 110:195–206. https://doi.org/10.1016/j.apcatb.2011.09.001
4. Peña DA, Uphade BS, Smirniotis PG (2004) TiO_2-supported metal oxide catalysts for low-temperature selective catalytic reduction of NO with NH_3: I. evaluation and characterization of first row transition metals. J Catal 221:421–431. https://doi.org/10.1016/j.jcat.2003.09.003
5. Kapteijn F, Singoredjo L, Andreini A, Moulijn JA (1994) Activity and selectivity of pure manganese oxides in the selective catalytic reduction of nitric oxide with ammonia. Appl Catal B Environ 3:173–189. https://doi.org/10.1016/0926-3373(93)E0034-9
6. Meng D, Zhan W, Guo Y et al (2015) A highly effective Catalyst of Sm-MnO_x for the NH_3-SCR of NO_x at low temperature: Promotional Role of Sm and its Catalytic performance. ACS Catal 5:5973–5983. https://doi.org/10.1021/acscatal.5b00747
7. Guo J, Li CT, Lu P et al (2011) Research on SCR denitrification of MnO_x/Al_2O_3 modified by CeO_2 and its mechanism at low temperature. Huanjing Kexue/Environmental Sci 32:2240–2246
8. Wu Z, Jiang B, Liu Y et al (2007) Experimental study on a low-temperature SCR catalyst based on MnO_x/TiO_2 prepared by sol-gel method. J Hazard Mater 145:488–494. https://doi.org/10.1016/j.jhazmat.2006.11.045
9. Qi G, Yang RT, Chang R (2003) Low-temperature SCR of NO with NH_3 over USY-Supported Manganese Oxide-Based catalysts. Catal Lett 87:67–71. https://doi.org/10.1023/A:1022809328087
10. Tang XL, Hao JM, Yi HH et al (2007) Selective catalytic reduction of NO_x with NH_3 by monolithic catalyst MnO_xAC/C under low temperature in the presence of excess O_2. Zhongguo Huanjing Kexue/China Environ Sci 27:845–850
11. Shen BX, Liu T, Zhao N et al (2012) Research of Catalytic Performance over Transition Metal Modified MnO_x-CeO_x/ACF Catalysts. Adv Mater Res 383–390:1945–1950. https://doi.org/10.4028/www.scientific.net/AMR.383-390.1945
12. Wu B, Liu X, Xiao P, Wang S (2008) TiO_2-Supported Binary Metal Oxide catalysts for low-temperature selective Catalytic reduction of NO_x with NH_3. Chem Res Chinese Univ 24:615–619. https://doi.org/10.1016/S1005-9040(08)60129-4
13. Nova I, Lietti L, Tronconi E, Forzatti P (2000) Dynamics of SCR reaction over a TiO_2-supported vanadia-tungsta commercial catalyst. Catal Today 60:73–82. https://doi.org/10.1016/S0920-5861(00)00319-9
14. Apostolescu N, Geiger B, Hizbullah K et al (2006) Selective catalytic reduction of nitrogen oxides by ammonia on iron oxide catalysts. Appl Catal B Environ 62:104–114. https://doi.org/10.1016/j.apcatb.2005.07.004
15. Kobayashi M, Hagi M (2006) V_2O_5-WO_3/TiO_2-SiO_2-SO_4^{2-} catalysts: influence of active components and supports on activities in the selective catalytic reduction of NO by NH_3 and in the oxidation of SO_2. Appl Catal B Environ 63:104–113. https://doi.org/10.1016/j.apcatb.2005.09.015
16. Chen JP, Yang RT (1992) Role of WO_3 in mixed V_2O_5-WO_3/TiO_2 catalysts for selective catalytic reduction of nitric oxide with ammonia. Appl Catal A Gen 80:135–148. https://doi.org/10.1016/0926-860X(92)85113-P
17. Shan W, Liu F, He H et al (2012) A superior Ce-W-Ti mixed oxide catalyst for the selective catalytic reduction of NO_x with NH_3. Appl Catal B Environ 115–116:100–106. https://doi.org/10.1016/j.apcatb.2011.12.019
18. Napolitano P, Liotta LF, Guido C et al (2022) Insights of Selective Catalytic Reduction Technology for Nitrogen Oxides Control in Marine Engine Applications. Catalysts 12:. https://doi.org/10.3390/catal12101191
19. Inorganic Crystal Structure Database (ICSD) (2014) ; FIZ Karlsruhe, GmbH: Eggenstein-Leopoldshafen, Germany, 2014
20. Liu W, Long Y, Zhou Y et al (2022) Excellent low temperature NH_3-SCR and NH_3-SCO performance over Ag-Mn/Ce-Ti catalyst: evaluation and characterization. Mol Catal 528:112510. https://doi.org/10.1016/j.mcat.2022.112510
21. Tang X, Li Y, Huang X et al (2006) MnO_x-CeO_2 mixed oxide catalysts for complete oxidation of formaldehyde: Effect of preparation method and calcination temperature. Appl Catal B Environ 62:265–273. https://doi.org/10.1016/j.apcatb.2005.08.004
22. Zhuang K, Qiu J, Tang F et al (2011) The structure and catalytic activity of anatase and rutile titania supported manganese oxide catalysts for selective catalytic reduction of NO by NH_3. Phys Chem Chem Phys 13:4463–4469. https://doi.org/10.1039/C0CP02288H
23. Qi G, Yang RT (2003) Performance and kinetics study for low-temperature SCR of NO with NH_3 over MnO_x-CeO_2 catalyst. J Catal 217:434–441. https://doi.org/10.1016/S0021-9517(03)00081-2
24. Cao L, Wu X, Chen Z et al (2019) A comprehensive study on sulfur tolerance of niobia modified CeO_2/WO_3-TiO_2 catalyst for low-temperature NH_3-SCR. Appl Catal A Gen 580:121–130. https://doi.org/10.1016/j.apcata.2019.05.007
25. Reiche MA, Maciejewski M, Baiker A (2000) Characterization by temperature programmed reduction. Catal Today 56:347–355. https://doi.org/10.1016/S0920-5861(99)00294-1
26. Gil S, Garcia-Vargas JM, Liotta LF et al (2015) Catalytic oxidation of propene over pd catalysts supported on CeO_2, TiO_2, Al_2O_3 and M/Al_2O_3 oxides (M = ce, Ti, Fe, Mn). Catalysts 5:671–689. https://doi.org/10.3390/catal5020671
27. Ousmane M, Liotta LF, Di Carlo G et al (2011) Supported au catalysts for low-temperature abatement of propene and toluene, as model VOC_s: support effect. Appl Catal B Environ 101:629–637. https://doi.org/10.1016/j.apcatb.2010.11.004
28. Thirupathi B, Smirniotis PG (2012) Nickel-doped Mn/TiO_2 as an efficient catalyst for the low-temperature SCR of NO with NH_3: Catalytic evaluation and characterizations. J Catal 288:74–83. https://doi.org/10.1016/j.jcat.2012.01.003
29. Gao C, Shi JW, Fan Z et al (2018) "Fast SCR" reaction over Sm-modified MnO_x-TiO_2 for promoting reduction of NO_x with NH_3. Appl Catal A Gen 564:102–112. https://doi.org/10.1016/j.apcata.2018.07.017
30. Komornicki S, Radecka M, Sobas P (2004) Structural properties of TiO_2 ± WO_3 thin ® lms prepared by r. f. sputtering. Mater Sci 5:527–531
31. Mdlovu NV, Yang NC, Lin KS et al (2022) Formulation and characterization of W-doped titania nanotubes for adsorption/photodegradation of methylene blue and basic violet 3 dyes. Catal Today 388–389:36–46. https://doi.org/10.1016/j.cattod.2021.03.015
32. Hu J, Lei Y, Yuan M et al (2020) Enhanced photoelectric performance of GQDs anchored WO_3 with a "dot-on-nanoparticle" structure. Mater Res Express 7:75602. https://doi.org/10.1088/2053-1591/aba393
33. Zhang W, Qi S, Pantaleo G, Liotta LF (2019) WO_3-V_2O_5 active oxides for NO_x SCR by NH_3: Preparation methods, catalysts' composition, and deactivation mechanism—A review. Catalysts 9. https://doi.org/10.3390/catal9060527
34. Imanari M, Watanabe Y, Matsuda S, Nakajima F (1981) Reduction of nox in combustion flue gases on tungsten based catalysts. Stud Surf Sci Catal 7:841–852. https://doi.org/10.1016/S0167-2991(08)64697-2
35. Kobayashi M, Miyoshi K (2007) WO_3-TiO_2 monolithic catalysts for high temperature SCR of NO by NH_3: influence of preparation

method on structural and physico-chemical properties, activity and durability. Appl Catal B Environ 72:253–261. https://doi.org/10.1016/j.apcatb.2006.11.007

36. Zhu J, Gao F, Dong L et al (2010) Studies on surface structure of $M_xO_y/MoO_3/CeO_2$ system (M = ni, Cu, Fe) and its influence on SCR of NO by NH_3. Appl Catal B Environ 95:144–152. https://doi.org/10.1016/j.apcatb.2009.12.021
37. Roy S, Hegde MS, Madras G (2009) Catalysis for NO_x abatement. Appl Energy 86:2283–2297. https://doi.org/10.1016/j.apenergy.2009.03.022
38. Shin Y, Jung Y, Cho CP et al (2020) NO_x abatement and N_2O formation over urea-SCR systems with zeolite supported Fe and Cu catalysts in a nonroad diesel engine. Chem Eng J 381:122751. https://doi.org/10.1016/j.cej.2019.122751